PLOS ONE

RESEARCH ARTICLE

A novel approach to quantify metrics of upwelling intensity, frequency, and duration

Amieroh Abrahams[1]*, **Robert W. Schlegel**[2], **Albertus J. Smit**[1,3]

1 Department of Biodiversity and Conservation Biology, University of the Western Cape, Cape Town, South Africa, **2** Department of Oceanography, Dalhousie University, Halifax, NS, Canada, **3** South African Environmental Observation Network, Elwandle Coastal Node, Port Elizabeth, South Africa

* amierohabrahams@gmail.com

Citation: Abrahams A, Schlegel RW, Smit AJ (2021) A novel approach to quantify metrics of upwelling intensity, frequency, and duration. PLoS ONE 16(7): e0254026. https://doi.org/10.1371/journal.pone.0254026

Editor: João Miguel Dias, Universidade de Aveiro, PORTUGAL

Received: March 25, 2021

Accepted: June 17, 2021

Published: July 8, 2021

Data Availability Statement: The analyses and data used in this paper maybe found at https://github.com/AmierohAbrahams/Upwelling_MCS.

Funding: Professor A.J Smit recieved fund from the South African National Research Foundation, reference number: ESS180920360856. The funder had no input in the study design, data, analysis, decision to publish or the preparation of the manuscript.

Competing interests: The authors have declared that no competing interests exist.

Abstract

The importance of coastal upwelling systems is widely recognized. However, several aspects of the current and future behaviors of these systems remain uncertain. Fluctuations in temperature because of anthropogenic climate change are hypothesized to affect upwelling-favorable winds and coastal upwelling is expected to intensify across all Eastern Boundary Upwelling Systems. To better understand how upwelling may change in the future, it is necessary to develop a more rigorous method of quantifying this phenomenon. In this paper, we use SST data and wind data in a novel method of detecting upwelling signals and quantifying metrics of upwelling intensity, duration, and frequency at four sites within the Benguela Upwelling System. We found that indicators of upwelling are uniformly detected across five SST products for each of the four sites and that the duration of those signals is longer in SST products with higher spatial resolutions. Moreover, the high-resolution SST products are significantly more likely to display upwelling signals at 25 km away from the coast when signals were also detected at the coast. Our findings promote the viability of using SST and wind time series data to detect upwelling signals within coastal upwelling systems. We highlight the importance of high-resolution data products to improve the reliability of such estimates. This study represents an important step towards the development of an objective method for describing the behavior of coastal upwelling systems.

1. Introduction

Eastern Boundary Upwelling Systems (EBUS) are characterized as vast regions of coastal ocean occurring along the western shores of continents bordering the Pacific and Atlantic Oceans [1–4]. Coastal upwelling associated with EBUS is known to have a large influence on the associated ecosystem's primary productivity, and hence the abundance, diversity, distribution, and production of marine organisms at all trophic levels [3–10]. Changes in the upwelling process over time is hypothesized to be strongly affected by anthropogenic climate change. According to the 'Bakun hypothesis', an increase in greenhouse gases facilitate an increase in daytime warming and night-time cooling and ultimately cause an increase in temperature gradients which will form stronger atmospheric pressure gradients [1, 11, 12]. These pressure gradients modulate the winds which ultimately affect the intensity and duration of upwelling [3,

9, 12–17]. Because changes in SST indirectly affect coastal ecosystems and have considerable, often far-reaching economic impacts [2, 3, 18–20], a better understanding of which SST products can most accurately detect upwelling will be important for any studies looking to identify and understand long-term changes to this phenomenon in EBUS [9, 15, 12, 17, 21, 22].

Previous attempts at identifying upwelling 'events' have employed a variety of approaches and incorporating an assortment of coastal temperature and wind variables and Ekman processes to estimate occurrences of upwelling, for example, Fielding and Davis [23] used a combination of wind speed, wind direction, and the orientation of the coast to calculate an alongshore wind component to quantify upwelling occurrences off the Western Cape coast of South Africa. Pfaff et al. [24] derived an upwelling index by contrasting offshore and onshore bottom temperatures in the southern Benguela region. Lamont et al. [25] used wind vectors to quantify upwelling variability along the same coastal region. More recently, El Aouni et al. [26] Used SST and wind data together with image processing techniques to detect and quantify upwelling signals. Several other authors made use of various other techniques to determine upwelling signals such as; Cury and Roy [27]; Demarcq and Faure [28]; Rossi et al., [29]; Benazzouz et al. [30] and Jacox et al. [31]. These examples primarily relied on wind data [11] to act as their main determinant for potential upwelling occurrences, rather than SST data. While wind patterns can act as a strong correlate for the presence of upwelling in many cases [11, 27]. SST data should arguably be more effective as these indicate presence of cold water of deep origin on the sea's surface. However, until recently, SST data were limited in several regards concerning data quality and quantity [32–34].

SST is regarded as one of the most important variables in the coupled ocean-atmosphere system and is a particularly useful research tool in the scientific fields of meteorology and oceanography [35–42]. For over 150 years, SST data have been collected using *in situ* measurement techniques [32] with satellite measurements of SST being available since the late 1970s [43–47]. Over the past decade, techniques have been developed to allow the assimilation and blending of different SST datasets from various *in situ* and satellite platforms. These are referred to as the Level-3 and Level-4 high resolution products, with the Level-4 data being gap-free [34], and are being widely applied in studies of coastal areas [48–51]. Previous studies demonstrated that satellite-based SST data are less accurate than *in situ* data due to the complexity of the oceanic and atmospheric conditions that need to be accounted for in deriving satellite SST products [52–56] and such errors vary both regionally and temporally [57]. However, in comparison to *in situ* temperature measurements collected from ships or buoys, a major advantage of satellite SST is their global coverage and near real time availability. SST datasets with a high level of accuracy, spatial consistency and completeness, and fine-scale resolution are necessary for weather and climate forecasting and are of great importance for reliable climate change monitoring [9, 12, 17, 34, 45, 51, 58–61].

For many applications, SST data are not used or provided at the full resolution of the sensors but are averaged over defined areas to produce a gridded product [45, 62]. Gridding in this way destroys more detailed information and as a result a gridded SST measurement is taken as an estimate of the average SST across a specific grid cell over a certain time. Small-scale features can evolve during the day, but the sensor sampling during this time is not dense enough for the sub-daily global analyses at a high spatial resolution [47, 63]. Furthermore, considering that the satellites are passing overhead only once every ~24 hours, images are only captured at very specific times during the day. To capture these small-scale features in a gridded analysis, it is suggested that the development of an improved analysis would have high resolution at small-scale features in regions of good coverage and lower resolution in areas of poor coverage [47].

Here, we aimed to test the utility of a new method for detecting upwelling signals and characterizing them in terms of intensity, frequency, and duration of upwelling events in an objective manner. Our approach is analogous to the marine heatwave methodology proposed by Hobday et al. [64]—in fact, it uses the same algorithm. By assessing increases in south easterly wind with concomitant decreases in coastal SST we can more reliably estimate the likelihood of an upwelling event. Given the importance of upwelling to the coastal productivity [65, 66], regional climate, and marine ecology, the ability to measure upwelling metrics such as the frequency, duration, and intensity of upwelling signals—in addition to the occurrence of the signals itself—allows us to quantify patterns of upwelling dynamics over time, in a manner that offers the potential to link these metrics to measures of ecosystem function. Furthermore, since the resultant increase in global temperature driven by climate change has a direct influence upon increase in global SST and will also manifest in changes in the upwelling process, being able to use a variety of metrics to subject to trend analysis in upwelling will be important for ecosystem management decisions.

To this end, this study aimed to observe patterns and trends in upwelling signals in the Benguela Upwelling System (BUS) across a range of localities and spatial scales off the South African West Coast. The BUS is divided into the northern (NBUS) and southern Benguela Upwelling Systems (SBUS) by a zone of intense perennial upwelling activity in Lüderitz within the Namibian region [25, 26, 67–69]. Meteorologically these regions are distinct. In the south, wind- induced upwelling reaches a maximum during spring and summer, whereas the northern region exhibits relatively less seasonal variation [67, 70–72]. Coastal upwelling commonly occurs between Cape Agulhas, in the south, to southern Angola in the north. We selected the SBUS upwelling system for this study because this physical process provides a strong seasonal signal of increasing and decreasing SST that is strongly localized to known centers of upwelling, and which relates to the coastal wind field that drives the offshore advection of water mass [71–73]. We apply our new method for identifying upwelling signals to data representative of this region. Because upwelling is such a well-characterized oceanographic process, the resultant fluctuating SST signal should be observed across independent SST products. Here we assess blended SST products covering a range of spatial grid resolutions from $0.05^{\circ} \times 0.05^{\circ}$ to $0.25^{\circ} \times 0.25^{\circ}$. We hypothesized that the higher resolution data should have a greater fidelity at detecting these upwelling signals, some of which might only be confined to smaller spatial scales or localized closer to the shore.

2. Materials and methods

2.1. Site description

The western region of the South African coastline is dominated by the Benguela Current, which forms the foundation of the Benguela Upwelling System (BUS) [74], and provides a natural laboratory for this study. Seasonal upwelling is controlled by south-easterly trade winds, with intense upwelling occurring throughout the summer months. This creates distinct temperature variations with much lower temperatures within the upwelling cells over a narrow continental shelf from the Cape Peninsula to Cape Columbine. To assess upwelling within the BUS, four sites from the South African Coastal Temperature Network (SACTN) dataset [61, 75] were selected as points of comparison (see below). Each site was situated along the West Coast of South Africa, and shore normal transects were used to sample the data at 0, 25 and 50 kms (Fig 1). Where 0 km pixels were those closest to their corresponding *in situ* site.

Upwelling processes in the southern Benguela are highly influenced by bottom topography [76]. The continental shelf that forms the eastern boundary of the Cape Basin, defined roughly by the 200 m isobath, varies in width from 10 km at prominent capes to 150 km near Port

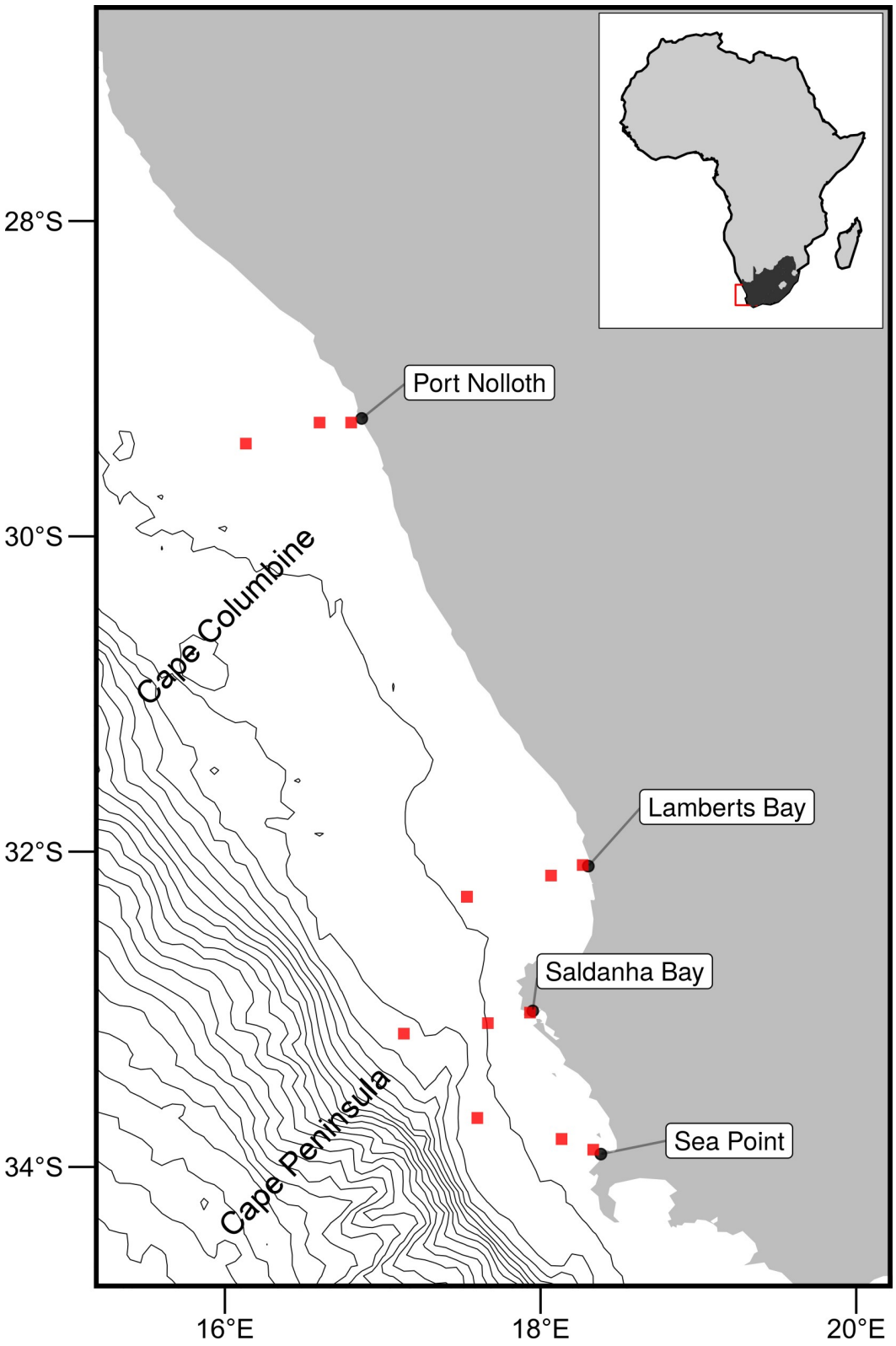

Fig 1. Map of the western portion of southern Africa showing the coastal bathymetry of the southern BUS. The black points represent the location of the *in situ* temperature recorders, and the red boxes show the pixels used along the shore normal transect from the satellite sea surface temperatures (SST) time series. The red boxes are at 0 km, 25 km and 50 km from the shoreline.

https://doi.org/10.1371/journal.pone.0254026.g001

Nolloth. In the vicinity of the Cape Peninsula and Cape Columbine, the coastline is irregular, and two canyons associated with these features cut into the shelf, parallel to the coast [76]. The dynamic topography of the area is such that the Agulhas Current water is fed into the Benguela systems from south of the Agulhas Bank. Upwelling in the BUS occurs in several distinct upwelling cells that form at locations of maximum wind stress curl, and where there is a change in the orientation of the coastline. Lutjeharms and Meeuwis [77] distinguished eight different cells: Cunene, Namibia, Walvis Bay, Lüderitz, Namaqua, Columbine, Cape Peninsula, and the Agulhas cell. Shannon and Nelson [78] included three more upwelling cells along the south coast. Given that this research study is restricted to the southern Benguela, discrete upwelling cells at Cape Columbine and the Cape Peninsula will be discussed [76]. The Cape Columbine and Cape Peninsula upwelling cells are identified as two distinct bands of cold water on the inner and mid-continental shelves at a depth of 0–100 m, where upwelling is generally more intense during summer [76]. This cold water is apparent along the length of the inner (0–100 m) and mid-continental (100–200 m) shelves [79]. In the Cape Peninsula region, a change in Sea Surface Temperature (SST) is present at Port Nolloth notably owing to the combined effects of being at the point of the southern limit of the Cape Peninsula upwelling cell and the sudden broadening of the inner shelf immediately to the south of the Peninsula.

2.2. Datasets

This study uses four Level-4 remotely sensed temperature datasets compiled by several organizations. Product 1 is the AVHRR-only (Advanced Very High-Resolution Radiometer) Optimally Interpolated Sea Surface Temperature (OISST) dataset, which has been providing global SST for nearly four decades [80]. OISST is a global $0.25^\circ \times 0.25^\circ$ gridded daily SST product that assimilates both remotely sensed and in situ sources of data to create a gap-free product [81]. The second product is the Group for High Resolution Sea Surface Temperature (GHRSST) Canadian Meteorological Center (CMC) Level-4 $0.2^\circ \times 0.2^\circ$ version 2; it combines infrared satellite SST at numerous points in the time series from the AVHRR, the European Meteorological Operational-A (METOP-A) and Operational-B (METOP-B) platforms, as well as the microwave SST data from the Advanced Microwave Scanning Radiometer 2 in conjunction with in situ observations of SST from ships and buoys from the ICOADS program. The third dataset is the Multi-scale Ultra-high Resolution (MUR) SST Analysis, which is produced using satellite instruments with datasets spanning 1 June 2002 to present times. MUR provides SST data at a spatial resolution of $0.01^\circ \times 0.01^\circ$ and is currently among the highest resolution SST datasets available. The final dataset is the GHRSST analysis produced daily using a multi-scale two-dimensional variational (MS-2DVAR) blending algorithm on a global 0.01° grid known as G1SST. This product uses satellite data from a variety of sensors, such as AVHRR, the Advanced Along Track Scanning Radiometer (AATSR), the Spinning Enhanced Visible and Infrared Imager (SEVIRI), the Moderate Resolution Imaging Spectroradiometer (MODIS), and in situ data from drifting and moored buoys. We acknowledge that not all products are completely independent as they share the use of AVHRR SST data, but the amount of subsequent blending, the incorporation of other SST data sources, the different blending and interpolation approaches used, and the differing final grid resolutions make them acceptably different for this study.

These SST products are compared against in situ temperature records from the South African Coastal Temperature Network (SACTN). This dataset consists of coastal seawater temperatures at 129 sites along the South African coastline, measured daily from 1972 until 2017 [61, 75]. Of these, 80 were measured using hand-held thermometers and the remaining 49 were measured using underwater temperature recorders (UTRs). For this analysis, the data were

combined and formatted into standardized comma separated values (CSV) files which allowed for a fixed methodology to be used across the entire dataset. In situ SST measurements were collected using a thermometer at a depth of 0 m for the four sites used in this study. The objective of this study was to identify upwelling signals using a variety of separate SST products for the period between 2011-01-01 to 2016-12-31. We specifically selected this range of years as they provide a sufficient overlap in time series between four remotely sensed SST and in situ datasets thereby offering candidate years for points of comparison.

An advantage to using in situ data over satellite data is that they may provide a more realistic representation of the thermal properties closer to the coast, whereas satellite data fail to accurately capture and represent temperature properties within the same spatial context. The result is that in situ data may be better at explaining upwelling signals within the coastal inshore environment. Further, evidence by Smit et al. [54] has shown that satellite data along the South African coastline may have a warm bias as much as 6˚C greater than in situ temperatures within the nearshore. Time series for each of the remotely sensed SST data products were created at the nearest pixel to each in situ station, and at each pixel along the shore-normal transects from these stations at 25 and 50 km from the coast (Fig 1). Wind speed and direction data were provided by the South African Weather Service (SAWS) at a three-hour resolution. The wind stations closest to each of the in situ stations were used to calculate the upwelling index (see below).

2.3. Defining and detecting upwelling

To detect and analyze upwelling at the four sites within the BUS, it was first necessary to define when upwelling occurred. To accomplish this, a set of threshold values for identifying when the phenomenon was taking place was required. For the wind component, we parsed alongshore, wind events at each site. We limited this to only include alongshore winds stronger than 5 $m.s^{-1}$ [11, 27]. since upwelling tends to only occur when wind exceeds the above speeds. We then used several parameters of those winds to inform an upwelling index calculated using the formula presented by Fielding and Davis [32]:

$$upwelling\ index = \mu(cos\theta - 160)$$

where μ represents the wind speed (m/s), θ represents the wind direction in degrees, and 160 is the orientation of the west coast in degrees [82]. The above equation produces a value called the 'upwelling index'. An upwelling index < 0 represents downwelling whilst an upwelling index > 0 represents upwelling [32]. For the temperature component, we evaluated coincidental drops in SST at each site when the upwelling index was greater than 0. If temperature dropped to the seasonally varying 25^{th} percentile of SST for a particular site, we deemed this as confirmation of the occurrence of an upwelling event at that site. See Schlegel et al. [61] for a similar threshold used to detected marine heatwaves and coldspells. with these thresholds established, it was then necessary to identify the number of consecutive days that must be exceeded for an upwelling signal to qualify as a discrete event. It must be noted that upwelling is known to vary on a seasonal basis and may also occur hourly (sub-daily). Therefore, the minimum duration for the classification of an upwelling signal was set as one day, the rationale being that data from the SACTN dataset as well as the satellite remotely sensed SST data are collected only at a daily resolution, preventing a temporally finer definition. With the upwelling index, SST data, and duration for an upwelling signal established, the detect_event() function from the **heatwaveR** package [83] was used to calculate metrics for the upwelling signals. Because upwelling signals were calculated relative to percentile exceedances, rather than a fixed temperature threshold, upwelling signals could occur any time of the year; however,

upwelling was shown to be more dominant during summer months (December, January, and February), as expected. This method of determining upwelling signals is novel as it considers both SST and wind parameters, and provides us with a descriptive statistical output, which include three metrics that define the properties of each of the signals detected (Table 1).

ANOVAs were used to compare the upwelling metrics against three main effects: *site*, *product*, and *distance*. Upwelling metrics as a function of satellite product type were assessed using *product* as the main effect, and nesting *distance* within *site*. To establish whether differences existed between sites or distances from the shore, the upwelling metrics were assessed as a function of *site* or *distance* independently for each satellite. Restrictions to experimental design prevented testing interaction effects within *product* types. These analyses sought to test if significant differences occurred between sites and data products. A Pearson product moment correlation was used to identify if the same upwelling signal detected at 0 km from the coastline were also regularly detected at 25 and 50 km from the coastline. The signals were classified by start and end date within the same data product. Thereafter, the average numbers of upwelling signals detected by each individual data product across all sites were compared using an ANOVA test. Thereafter, a Chi-square analysis was used to compare of the number of upwelling signals detected when including and excluding an SST filter when determining upwelling signals.

3. Results

One-way ANOVA indicated no significant difference in upwelling duration between sites across each respective data product: SACTN (d.f. = 3, $F = 5.91$, $p > 0.05$), OISST (d.f. = 3, $F = 0.12$, $p > 0.05$), CMC (d.f. = 3, $F = 0.57$, $p > 0.05$), MUR (d.f. = 3, $F = 2.50$, $p > 0.05$) and G1SST (d.f. = 3, $F = 0.64$, $p > 0.05$) (Fig 2A) products. The Sea Point site displayed the longest mean duration of upwelling signals. Lamberts Bay had the shortest duration upwelling signals. Particularly, the Lamberts Bay data from the SACTN dataset showed the shortest duration upwelling signals.

A significant difference was found in mean intensity of upwelling between sites in the OISST (d.f. = 3, $F = 5.82$, $p < 0.001$) and SACTN (d.f. = 3, $F = 7.39$, $p < 0.001$) products. Conversely, no significant difference was found in the CMC (d.f. = 3, $F = 1.04$, $p > 0.05$), MUR (d.f. = 3, $F = 2.48$, $p > 0.05$) and G1SST (d.f. = 3, $F = 2.66$, $p > 0.05$) products (Fig 2B). There was no significant difference in cumulative intensity of upwelling between sites in the CMC (d.f. = 3, $F = 0.58$, $p = 0.62$) (Fig 2C). The mean intensity of upwelling signals was highest in Saldanha Bay and Sea Point for the MUR and G1SST data. We found that there was a significant difference between cumulative intensity of upwelling signals between sites only when using the SACTN dataset. The cumulative intensity of upwelling signals was most intense in Saldanha Bay and Sea Point for all of the products.

An ANOVA showed no significant difference in the duration of upwelling signals detected at different distances from the shore during the summer season in the CMC (d.f. = 2, $F = 1.03$, $p = 0.35$) and G1SST (d.f. = 2, $F = 2.55$, $p > 0.05$) products. However, a significant difference was present across the MUR (d.f. = 2, $F = 3.33$, $p < 0.05$) and OISST data (d.f. = 2, $F = 5.17$,

Table 1. Metrics of upwelling signals and their descriptions.

Name (unit)	Definition
Count (*n*)	Number of upwelling signals per year
Mean intensity (˚C)	Mean temperature anomaly during the upwelling signal
Cumulative intensity (˚C.days)	Sum of the daily intensity anomalies over the duration of the signal

https://doi.org/10.1371/journal.pone.0254026.t001

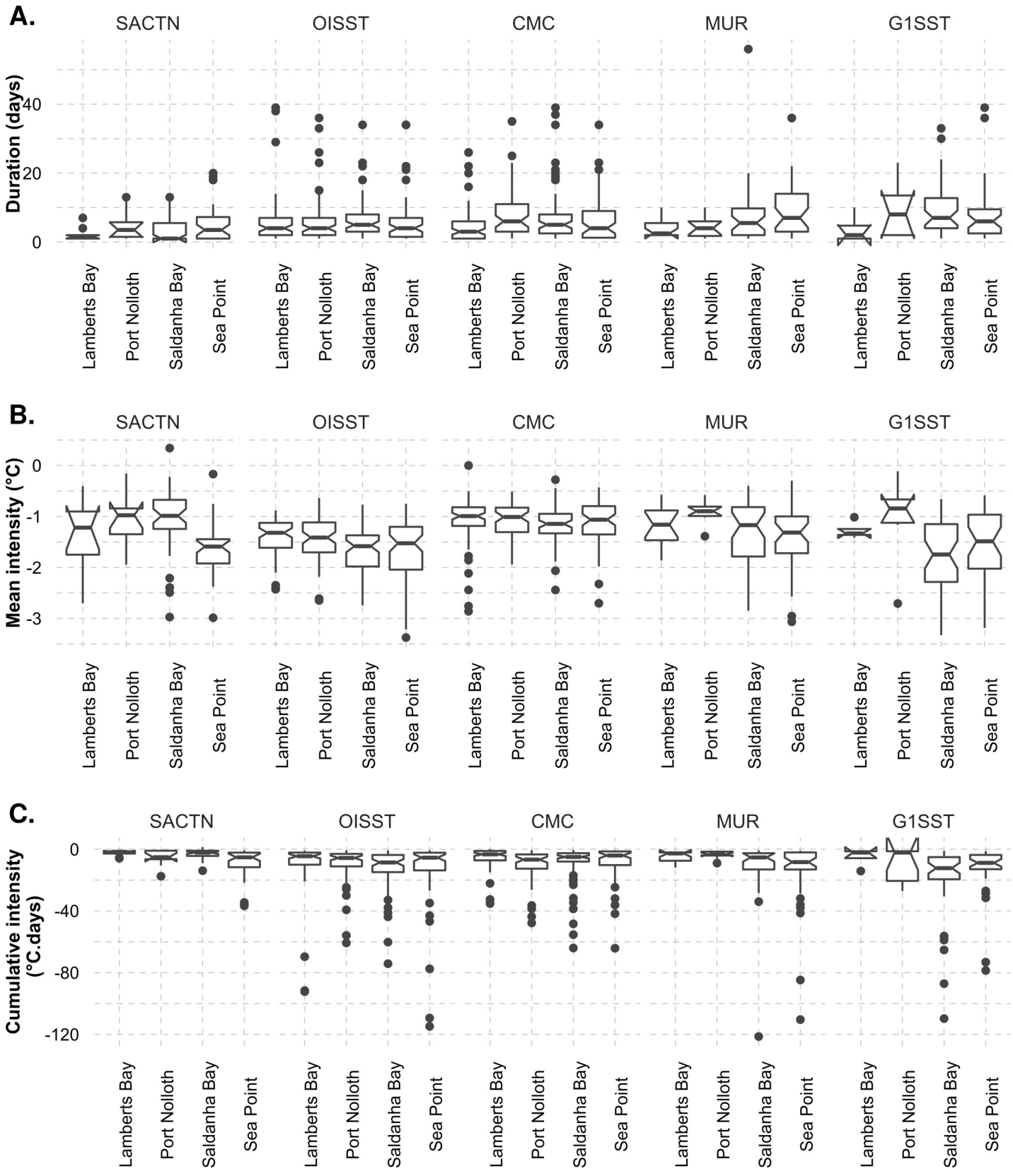
A.
SACTN
OISST
CMC
MUR
G1SST
Duration (days)
0
20
40
Lamberts Bay
Port Nolloth
Saldanha Bay
Sea Point
B.
SACTN
OISST
CMC
MUR
G1SST
Mean intensity (°C)
0
-1
-2
-3
Lamberts Bay
Port Nolloth
Saldanha Bay
Sea Point
C.
SACTN
OISST
CMC
MUR
G1SST
Cumulative intensity (°C.days)
0
-40
-80
-120
Lamberts Bay
Port Nolloth
Saldanha Bay
Sea Point

Fig 2. Boxplots showing the upwelling A) duration, B) mean intensity, and C) cumulative intensity for the upwelling signals detected with the four satellite products and the SACTN *in situ* collected data at the different sites during summer months (December, January, and February), over a six-year period. The lower and upper hinges correspond to the first and third quartiles, and outliers are shown as points. The notches offer a guide to significant difference in medians, *i.e.*, if the notches of two box plots overlap it suggests that there is no statistically significant difference between the medians being compared.

https://doi.org/10.1371/journal.pone.0254026.g002

$p < 0.05$) products. The MUR and G1SST often yielded the longest duration of upwelling signals at 0 and 25 km from the shore (Fig 3A).

Significant differences in the mean intensity of upwelling signals were present across different distances from the shore in the G1SST (d.f. = 2, $F = 15.38$, $p < 0.001$), MUR (d.f = 2, $F = 5.12$, $p < 0.001$) and OISST (d.f. = 2, $F = 5.17$, $p < 0.05$). MUR and G1SST products displayed the highest mean intensity of upwelling signals at 0 km from the coast (Fig 3B). The mean intensity of upwelling decreased further away from the coast in the higher resolution products.

A one-way ANOVA showed a significant difference in the cumulative intensity of upwelling signals detected at different distances from the shore in the G1SST (d.f. = 2, $F = 7.03$, $p < 0.05$) and MUR (d.f. = 2, $F = 4.69$, $p < 0.05$) data products. (Fig 3C). The CMC (d.f. = 2, $F = 0.33$, $p > 0.05$) and OISST (d.f. = 2, $F = 0.06$, $p > 0.05$) products showed no significant difference in cumulative intensity. The OISST, MUR and G1SST products yielded the highest cumulative intensity at 0 km from the coastline. The cumulative intensity of upwelling signals for all products decreased further from the coast. The results of a nested ANOVA showed that there was a significant difference in the duration of upwelling signals detected amongst the data products (nested ANOVA, d.f. = 3, $F = 3.01$, $p < 0.02$). The G1SST product had the longest duration of upwelling signals while the OISST products had the shortest. We found a significant difference in the mean intensity of upwelling signals between data products (nested ANOVA, d.f. = 3, $F = 49.93$, $p < 0.001$). The G1SST and MUR data products showed the highest mean intensity while CMC had the lowest. We also found a significant difference in the cumulative intensity of upwelling signals between the data products of different resolutions (nested ANOVA, d.f. = 3, $F = 5.71$, $p < 0.05$). The G1SST product showed the strongest cumulative intensity of upwelling and the CMC data the weakest.

Pearson correlation revealed the possibility of observing the same upwelling signal detected at 0, 25, and 50 km from the coast respectively varied across the individual data products at each of the four sites (Table 2). Overall, we found that upwelling occurred simultaneously at 0 km and at 25 km considerably more frequently than between 0 km and 50 km from the coastline. In addition, the likelihood of detecting upwelling signals at 50 km from the coastline were notably lower throughout all pairwise comparisons. The individual data products yielded different counts of upwelling signals at distances of 0 km, 25 km, and 50 km from the coastline. There was no significant difference between the number of upwelling signals collected at the different sites (one-way ANOVA: $F = 1.73$, d.f = 3, SS = 520, $p > 0.05$). However, there was a significant difference in the number of signals detected between products ($F = 146.611$, d.f = 3, SS = 40638, $p < 0.001$) and at different distances from the coastline ($F = 0.76$, d.f = 2, SS = 141, $p > 0.05$).

Comparisons of the number of upwelling signals detected when including and excluding SST data revealed that significantly more upwelling events were present across sites and data products when using only wind data (Table 3; $\chi^2 = 141.18$, $p < 0.001$). The results of Chi-squared test comparing the mean number of upwelling events between filtered and non-filtered counts per data product showed that on average the filtered data had lower numbers of upwelling events than expected when assessing each dataset individually. However, these differences in the count of upwelling events were only significant in all of the products (Table 3). Similarly, site-specific comparisons revealed that upwelling events at all sites showed

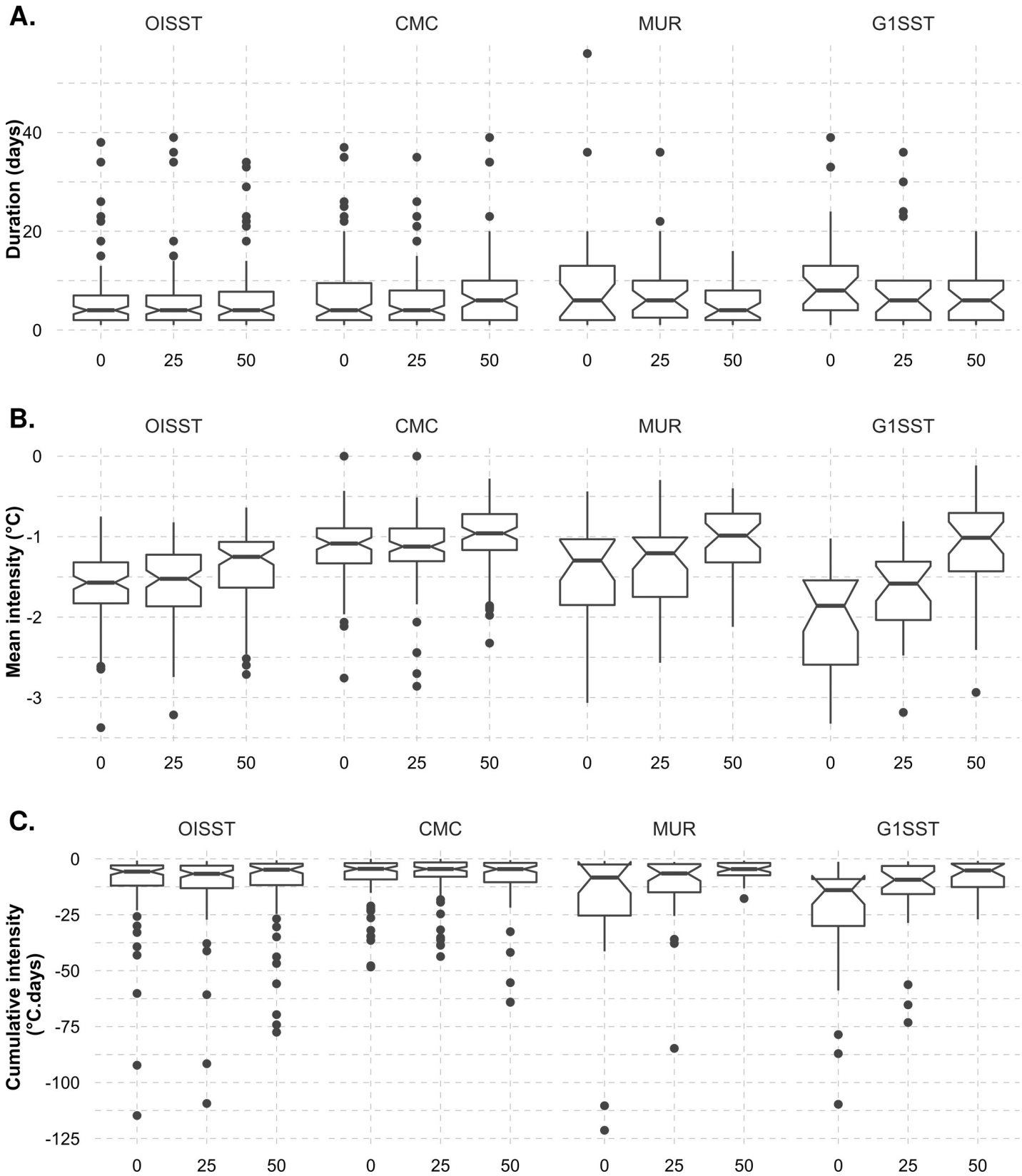

Fig 3. Boxplots showing the A) duration, B) mean intensity, and C) cumulative intensity for each of the upwelling signals detected at various distances (km) from the shore for the four satellite products during summer months (December, January, and February), over a six-year period. The properties of the boxplots are as in Fig 2.

https://doi.org/10.1371/journal.pone.0254026.g003

Table 2. A Pearson correlation of the relationship between the number of signals detected at 0 km versus a distance of 25 km and between the number of signals at 0 km and 50 km.

Product	Site	0 km vs 25 km	0 km vs 50 km
OISST	Port Nolloth	0.97 ****	0.52 ***
	Lamberts Bay	0.36	0.21*
	Saldanha Bay	0.91 ****	0.51***
	Sea Point	0.95 ***	0.73 **
CMC	Port Nolloth	0.95***	0.60**
	Lamberts Bay	0.48*	0.30**
	Saldanha Bay	0.47 ***	0.38**
	Sea Point	0.75 ****	0.33 ***
G1SST	Port Nolloth	0.75 ***	0.76***
	Lamberts Bay	0.68 **	0.57 **
	Saldanha Bay	0.44 **	0.33 *
	Sea Point	0.47 **	0.32 **
MUR	Port Nolloth	0.92 **	0.80
	Lamberts Bay	0.86 ****	0.76 **
	Saldanha Bay	0.70 *	0.62 *
	Sea Point	0.87 **	0.72 *

Significant levels are as follows

* $p \leq 0.05$

** $p \leq 0.01$

*** $p \leq 0.001$, and

**** $p \leq 0.0001$.

https://doi.org/10.1371/journal.pone.0254026.t002

significant differences between filtered and unfiltered counts of upwelling events, with unfiltered counts being notably higher in all cases.

4. Discussion

4.1. Detection of upwelling signals

Over the past few decades, upwelling has been mainly described and determined in general terms using a variety of upwelling indices derived from diverse combinations of wind, SST, and Ekman transport variables [2–26, 29–31, 84]. We demonstrate that our novel approach to

Table 3. Results of Chi-squared test comparing the numbers of upwelling signals detecting with and without SST as a filter across the four data products at four sites.

Comparison	$\chi 2$	p	d.f.
All products and sites	141.18	<0.001	1
OISST	15.77	<0.001	3
MUR	14.39	0.002	3
G1SST	20.04	<0.001	3
CMC	20.47	<0.001	3
SACTN	34.11	<0.001	3
Lamberts Bay	108.77	<0.001	4
Port Nolloth	152.45	<0.001	4
Saldanha Bay	90.41	<0.001	4
Sea Point	19.65	<0.001	4

https://doi.org/10.1371/journal.pone.0254026.t003

characterize upwelling events using SST in combination with wind variables to determine metrics that objectively and quantitatively describe the upwelling process offers a similarly versatile means for detecting changes in upwelling dynamics associated with climate change. We calculate a set of summary statistics (i.e., the metrics) for each upwelling 'signal,' including its intensity, duration, and frequency by making use of the marine heatwave algorithm [61, 64]. Time series of these metrics are intuitively understood and allow for upwelling signals to be uniquely described and compared across space and time, even between upwelling regions. The use of this approach is not independent on the nature of the data, and here we explore this for SST.

4.2. Data products

Our analysis showed that differences exist between SST products and sites when comparing the upwelling metrics. The highest resolution data, MUR and G1SST, which are available on a 0.01 grid, yielded the longest duration and cumulative intensity of upwelling signals compared to the coarser resolution data products. The MUR product consistently yielded upwelling signals of the greatest intensity. Upwelling signals were most intense at the shore in all the SST products. Analysis of the CMC and SACTN datasets revealed that signals did not often exceed a duration of 10 days, whereas in OISST, MUR and G1SST the signals were detected for up to 14 days and even longer in some rare cases. Moreover, most of the signals detected in CMC and SACTN products only lasted for three days. This was similar for the higher resolution data products (G1SST and MUR) which also showed a high prevalence of signals lasting for just four days. In most cases, the number of signals detected at 0 km was higher than the number of signals detected at 50 km for the data products with the highest resolution. We also noted differences in mean intensity between products and distances from the site. The highest number of signals detected were recorded in the OISST and CMC products. The results show that the use of wind data without corresponding SSTs is likely to produce exaggerated estimations of upwelling. However, by incorporating SST data allows for a greater chance of reducing type I errors, i.e., false positives for estimating upwelling and reducing the overall likelihood for erroneously claiming an upwelling event based on wind data alone when corresponding SST are not cooling.

Level-4 gridded SST datasets obtained from satellite imagery have provided an important understanding of offshore oceanographic processes. Their utility often stems from the fact that they are spatially complete. However, coastal features such as upwelling cells are often smaller than the highest resolution of most SST products [54]. In this study, estimates of upwelling duration, mean intensity and cumulative intensity may have been overestimated from data collected by the MUR and G1SST data products when comparing them to the in situ collected SACTN data. These products are more likely to be susceptible to errors relating to limitations and data collection biases associated with satellite-derived sampling [85, 86]. The overestimated metrics of upwelling may be due to errors from different sources which are produced at each of the successive data processing level [86]. SST accuracy refers to the retrieval error produced at Level-2 (derived SSTs at pixel bases), but Level-3 (binned, gridded, and averaged Level-2 values) and Level-4 fields are extensively used in climate and modeling studies, mainly because of the desirable features of being "gridded and gap-free" [86].

It is important to note that the data sources are intrinsically different in the ways in which they were obtained or recorded. Consequently, discrepancies between datasets are to be expected. For example, the SACTN in situ collected data will reflect the actual temperature of the water being measured but instrumental differences when using a thermometer or an electronic sensor will result in inconsistencies. This is particularly prevalent because satellite temperatures are collected remotely, and sensors do not contact the water. Smit et al. [54] showed

that warm and cold biases exist along the southern and western coastal region of South Africa, and the juncture between upwelling and non-upwelling regions tend to influence the variability and magnitude of the SST bias. While flagging techniques are supposed to occasionally flag 'good' values [87], it was found that flagging may occasionally be too vigorous for EBUS [88]. For example, the flagging method used on an OISST reference test induces warm coastal bias in data from both the MUR and G1SST data during summer [88]. It should be noted that this phenomenon can be explained by strong coastal SST gradients in these upwelling regions—here pixel-based corrections developed for oceanic applications often fail or are inappropriate due to the strong thermal gradients associated with upwelling.

Flagging techniques used to de-cloud data are also known to reduce strong biases at a monthly scale with strong horizontal SST gradients especially in upwelling systems [54]. Missing pixels at the land/sea edge or 'land bleed'—i.e., pixels not flagged as missing, but which are influenced by land temperatures 'mixing' with the actual sea temperatures, may also influence temperature data obtained. Contributing towards the magnitude of differences in upwelling signals detected between the different SST products are factors such as data resolution, proximity from the coastline, and the presence or absence of upwelling cells or embayments.

SST generally shows a high degree of correspondence with measurements obtained by buoys and other sources of in situ seawater temperature measurements [54, 89]. However, although SST products developed offshore and within the open ocean are being applied to the coastal regions, reports exist to inform users to exercise caution when using SST datasets in these coastal regions [90]. Many upwelling pulses may be localized and of short duration (i.e., lasting for a few hours or days; Duncan et al. [91], Sawall et al. [92]), which may contribute to the higher resolution (MUR and G1SST) products yielding more signals lasting for a longer period when compared to the coarser resolution products (e.g., OISST). Prior investigations for quantifying the durations of upwelling events across the globe have adopted several approaches and estimates derived using various methodologies. For example, Wang et al. [93] used wind driven Ekman transport indices to estimate that upwelling events in the southern hemisphere last fewer than 10 days on average. Contrastingly, Iles et al. [94] used PFEL indices to estimate upwelling duration as $>$ 6 days. Here we estimate upwelling as only lasting for 3–6 days on average, considerably shorter than previous estimates elsewhere. Both MUR and G1SST have a limited time series length (MUR: 2002-Jun-01 to Present, G1SST: 2010-Jun-09 to 2019-Dec-09) and for this reason are not well suited to climate change studies, which require time series of at least 30 years in duration. In this case, the OISST dataset would be more suitable. The adoption of a consistent definition and metrics for upwelling will facilitate comparisons between different upwelling signals, across seasons and at regional scales. It will also facilitate the comparison of observed signals against modelled projections, which will be useful in understanding future changes in upwelling signals. Confidence in the robust detection of upwelling signals will only be achieved with the use of high-quality datasets and a verifiable method.

4.3. Oceanography

At the latitude of the Cape Peninsula, cooler upwelled water ($<$14˚C) is confined primarily to the narrow inner shelf and this is evident in our data as we observe the most intense upwelling signals closer to the shore. It is also evident that the high resolution G1SST and MUR data sampled in Lamberts Bay, Saldanha Bay and Sea Point show the highest number of upwelling signals detected at the narrow inner shelf with fewer signals collected at the mid latitude shelf. Our findings further show that the coarser resolution (OISST) product fails to detect signals further offshore, as seen in Sea Point. Currie [95] and Hart and Currie [96] further explain

that the BUS consists of a series of anticyclonic eddies of interlocking cool and warm water, which is in a constant state of change. This allows for upwelling cells or patches, formed by water that originates from between 200 and 300 m deep, to not be uniform along the coast. By understanding the topography, it is evident that, although upwelling is not visible at the surface, subsurface upwelling is possible [76]. This further suggests that in cases when the same signal was detected at the shoreline and 25 km from the coast, a corresponding signal would not be identified at 50 km and this may be explained by sub-surface upwelling.

While the SST data may be satisfactory for interpretation of regional phenomena, they nevertheless suffer from several drawbacks when applied within the coastal region. Here the interaction of hydrodynamic and atmospheric forces creates a complex system which is influenced by larger variability at smaller spatial scales than further offshore [88]. Hydrodynamic regimes, such as stratified water columns, may break down at the coast in very shallow waters, and seawater temperatures measured there may not directly relate to SSTs sampled further from the coast at the ocean's surface [97]. This inshore hydrodynamics may be described by a) the injection of turbulence through breaking waves, thus increasing the breakdown of the mixed layer; b) convective mixing due to the cooling through the process of evaporation, which occurs during winter months under cool dry air; c) tidal mixing which minimizes the vertical thermal gradient; and d) mixing through velocity often caused by wind driven currents. Together, these processes homogenize the first few meters of the water column and therefore minimize the difference between the surface temperature and deeper bulk temperature [98]. In hydrodynamically active zones, such as the BUS, the absence of shallow stratification would cause a portion of cooler water than the bulk surface waters of the ocean to which satellite SSTs have been referenced. Thermal heating of coastal waters may also be exaggerated due to the proximity to the coast [88]. This type of heating is commonly seen in embayments, which reduce water exchange and limit wave activity and ultimately affect the deepening of the thermocline. These processes are highly variable on a spatial and temporal scale depending on the coastal bathymetry and wind regime.

5. Conclusions

Overall, in the rapidly changing climate, the detection, characterization, and prediction of upwelling signals will become increasingly important. The impact of climate change on upwelling is an emerging area of interdisciplinary research with potential for collaborative initiatives in understanding coupled phenomena across physical oceanographic, ecological, and socio-economic areas of inquiry. The metrics of upwelling that we introduce here—intensity, duration, and frequency of signals of upwelling—provide a consistent framework that lends itself to be quantitatively coupled to metrics of change indicative of aspects of the regional biology, ecological impacts, and trends in the societal aspects of stakeholders whose livelihoods and businesses are coupled with the functioning of upwelling systems. Our approach not only provides us with a new method of detecting upwelling signals, which is useful to observe trends in upwelling signals over time, but also emphasizes the importance of selecting the correct data product in concert with knowledge about the nature of the physical phenomena being studied.

Acknowledgments

The authors thank DAFF, DEA, KZNSB, EKZNW, SAWS, and SAEON for contributing all of the raw data used within the SACTN dataset. A special thanks to Jody Barends for assistance with preparing this manuscript.

Author Contributions

Conceptualization: Amieroh Abrahams, Albertus J. Smit.

Data curation: Amieroh Abrahams.

Formal analysis: Amieroh Abrahams, Robert W. Schlegel, Albertus J. Smit.

Funding acquisition: Albertus J. Smit.

Investigation: Amieroh Abrahams, Albertus J. Smit.

Methodology: Amieroh Abrahams, Robert W. Schlegel.

Project administration: Amieroh Abrahams.

Resources: Amieroh Abrahams.

Software: Amieroh Abrahams, Robert W. Schlegel.

Supervision: Robert W. Schlegel, Albertus J. Smit.

Visualization: Amieroh Abrahams, Albertus J. Smit.

Writing – original draft: Amieroh Abrahams, Robert W. Schlegel, Albertus J. Smit.

Writing – review & editing: Amieroh Abrahams, Robert W. Schlegel, Albertus J. Smit.

References

1. Bakun A. Global climate change and intensification of coastal ocean upwelling. Science. 1990 Jan 12; 247(4939):198–201. https://doi.org/10.1126/science.247.4939.198 PMID: 17813287
2. Pauly D, Christensen V. Primary production required to sustain global fisheries. Nature. 1995 Mar; 374 (6519):255–7.
3. Bakun A, Field DB, Redondo-Rodriguez AN, Weeks SJ. Greenhouse gas, upwelling-favorable winds, and the future of coastal ocean upwelling ecosystems. Global Change Biology. 2010 Apr; 16(4):1213–28.
4. Bakun A, Black BA, Bograd SJ, Garcia-Reyes M, Miller AJ, Rykaczewski RR, et al. Anticipated effects of climate change on coastal upwelling ecosystems. Current Climate Change Reports. 2015 Jun 1; 1 (2):85–93.
5. Barth JA, Menge BA, Lubchenco J, Chan F, Bane JM, Kirincich AR, et al. Delayed upwelling alters nearshore coastal ocean ecosystems in the northern California current. Proceedings of the National Academy of Sciences. 2007 Mar 6; 104(10):3719–24. https://doi.org/10.1073/pnas.0700462104 PMID: 17360419
6. Messié M, Ledesma J, Kolber DD, Michisaki RP, Foley DG, Chavez FP. Potential new production estimates in four eastern boundary upwelling ecosystems. Progress in Oceanography. 2009 Dec 1; 83(1–4):151–8.
7. Gruber N, Lachkar Z, Frenzel H, Marchesiello P, Münnich M, McWilliams JC, et al. Eddy-induced reduction of biological production in eastern boundary upwelling systems. Nature geoscience. 2011 Nov; 4 (11):787–92.
8. Pegliasco C, Chaigneau A, Morrow R. Main eddy vertical structures observed in the four major Eastern Boundary Upwelling Systems. Journal of Geophysical Research: Oceans. 2015 Sep; 120(9):6008–33.
9. Varela R, Álvarez I, Santos F, DeCastro M, Gómez-Gesteira M. Has upwelling strengthened along worldwide coasts over 1982–2010?. Scientific reports. 2015 May 8; 5(1):1–5. https://doi.org/10.1038/srep10016 PMID: 25952477
10. Brady RX, Lovenduski NS, Alexander MA, Jacox M, Gruber N. On the role of climate modes in modulating the air–sea CO 2 fluxes in eastern boundary upwelling systems. Biogeosciences. 2019 Jan 24; 16 (2):329–46.
11. García-Reyes M, Largier JL, Sydeman WJ. Synoptic-scale upwelling indices and predictions of phyto- and zooplankton populations. Progress in Oceanography. 2014 Jan 1; 120:177–88.
12. Varela R, Lima FP, Seabra R, Meneghesso C, Gómez-Gesteira M. Coastal warming and wind-driven upwelling: a global analysis. Science of the Total Environment. 2018 Oct 15; 639:1501–11. https://doi.org/10.1016/j.scitotenv.2018.05.273 PMID: 29929313

13. Hsieh WW, Boer GJ. Global climate change and ocean upwelling. Fisheries Oceanography. 1992 Dec; 1(4):333–8.

14. Mote PW, Mantua NJ. Coastal upwelling in a warmer future. Geophysical research letters. 2002 Dec; 29(23):53–1.

15. Patti B, Guisande C, Riveiro I, Thejll P, Cuttitta A, Bonanno A, et al. Effect of atmospheric CO2 and solar activity on wind regime and water column stability in the major global upwelling areas. Estuarine, Coastal and Shelf Science. 2010 Jun 10; 88(1):45–52.

16. Pardo PC, Padín XA, Gilcoto M, Farina-Busto L, Pérez FF. Evolution of upwelling systems coupled to the long-term variability in sea surface temperature and Ekman transport. Climate Research. 2011 Aug 30; 48(2–3):231–46.

17. Varela R, Rodríguez-Díaz L, de Castro M, Gómez-Gesteira M. Influence of Eastern Upwelling systems on marine heatwaves occurrence. Global and Planetary Change. 2021 Jan; 196:103379.

18. Murawski SA. Climate change and marine fish distributions: forecasting from historical analogy. Transactions of the American Fisheries Society. 1993 Sep 1; 122(5):647–58.

19. Costanza R, d'Arge R, de Groot R, Farber S, Grasso M, Hannon B, et al. 1997. The value of the world's ecosystem services and natural capital. Nature. 1997; 387:253–60.

20. Tretkoff E. Research Spotlight: Coastal cooling and marine productivity increasing off Peru. Eos, Transactions American Geophysical Union. 2011 May 24; 92(21):184–.

21. McGregor HV, Dima M, Fischer HW, Mulitza S. Rapid 20th-century increase in coastal upwelling off northwest Africa. science. 2007 Feb 2; 315(5812):637–9. https://doi.org/10.1126/science.1134839 PMID: 17272719

22. Narayan N, Paul A, Mulitza S, Schulz M. Trends in coastal upwelling intensity during the late 20th century. Ocean Science. 2010 Sep 22; 6(3):815–23.

23. Fielding PJ, Davis CL. Carbon and nitrogen resources available to kelp bed filter feeders in an upwelling environment. Marine Ecology Progress Series. 1989 Jul 27:181–9.

24. Pfaff MC, Branch GM, Wieters EA, Branch RA, Broitman BR. Upwelling intensity and wave exposure determine recruitment of intertidal mussels and barnacles in the southern Benguela upwelling region. Marine Ecology Progress Series. 2011 Mar 14; 425:141–52.

25. Lamont T, García-Reyes M, Bograd SJ, Van Der Lingen CD, Sydeman WJ. Upwelling indices for comparative ecosystem studies: Variability in the Benguela Upwelling System. Journal of Marine Systems. 2018 Dec 1; 188:3–16.

26. El Aouni A, Daoudi K, Minaoui K, Yahia H. Robust detection of the North-West African upwelling from SST images. IEEE Geoscience and Remote Sensing Letters. 2020 Apr 9.

27. Cury P, Roy C. Optimal environmental window and pelagic fish recruitment success in upwelling areas. Canadian Journal of Fisheries and Aquatic Sciences. 1989 Apr 1; 46(4):670–80.

28. Demarcq H, Faure V. Coastal upwelling and associated retention indices derived from satellite SST. Application to Octopus vulgaris recruitment. Oceanologica Acta. 2000 Aug 1; 23(4):391–408.

29. Rossi V, Feng M, Pattiaratchi C, Roughan M, Waite AM. On the factors influencing the development of sporadic upwelling in the Leeuwin Current system. Journal of Geophysical Research: Oceans. 2013 Jul 1; 118(7):3608–21.

30. Benazzouz A, Mordane S, Orbi A, Chagdali M, Hilmi K, Atillah A, et al. An improved coastal upwelling index from sea surface temperature using satellite-based approach–The case of the Canary Current upwelling system. Continental Shelf Research. 2014 Jun 15; 81:38–54.

31. Jacox MG, Edwards CA, Hazen EL, Bograd SJ. Coastal upwelling revisited: Ekman, Bakun, and improved upwelling indices for the US West Coast. Journal of Geophysical Research: Oceans. 2018 Oct; 123(10):7332–50.

32. Rayner NA, Brohan P, Parker DE, Folland CK, Kennedy JJ, Vanicek M, et al. Improved analyses of changes and uncertainties in sea surface temperature measured in situ since the mid-nineteenth century: The HadSST2 dataset. Journal of Climate. 2006 Feb 1; 19(3):446–69.

33. Lobdell DT, Jagai JS, Rappazzo K, Messer LC. Data sources for an environmental quality index: availability, quality, and utility. American journal of public health. 2011 Dec; 101(S1):S277–85.

34. Meneghesso C, Seabra R, Broitman BR, Wethey DS, Burrows MT, Chan BK, et al. Remotely-sensed L4 SST underestimates the thermal fingerprint of coastal upwelling. Remote Sensing of Environment. 2020 Feb 1; 237:111588.

35. Casey KS, Cornillon P. A comparison of satellite and in situ–based sea surface temperature climatologies. Journal of Climate. 1999 Jun; 12(6):1848–63.

36. Wentz FJ, Gentemann C, Smith D, Chelton D. Satellite measurements of sea surface temperature through clouds. Science. 2000 May 5; 288(5467):847–50. https://doi.org/10.1126/science.288.5467.847 PMID: 10797004

37. Mesias JM, Bisagni JJ, Brunner AM. A high-resolution satellite-derived sea surface temperature climatology for the western North Atlantic Ocean. Continental Shelf Research. 2007 Jan 15; 27(2):191–207.

38. Harlass J, Latif M, Park W. Improving climate model simulation of tropical Atlantic sea surface temperature: The importance of enhanced vertical atmosphere model resolution. Geophysical Research Letters. 2015 Apr 16; 42(7):2401–8.

39. Isachsen PE, Koszalka I, LaCasce JH. Observed and modeled surface eddy heat fluxes in the eastern Nordic Seas. Journal of Geophysical Research: Oceans. 2012 Aug; 117(C8).

40. Santos F, Gómez-Gesteira M, Varela R, Ruiz-Ochoa M, Días JM. Influence of upwelling on SST trends in La Guajira system. Journal of Geophysical Research: Oceans. 2016 Apr; 121(4):2469–80.

41. Vazquez-Cuervo J, Dewitte B, Chin TM, Armstrong EM, Purca S, Alburqueque E. An analysis of SST gradients off the Peruvian Coast: The impact of going to higher resolution. Remote Sensing of Environment. 2013 Apr 15; 131:76–84.

42. Vazquez-Cuervo J, Torres HS, Menemenlis D, Chin T, Armstrong EM. Relationship between SST gradients and upwelling off Peru and Chile: Model/satellite data analysis. International Journal of Remote Sensing. 2017 Dec 2; 38(23):6599–622.

43. Reynolds RW, Smith TM. Improved global sea surface temperature analyses using optimum interpolation. Journal of climate. 1994 Jun; 7(6):929–48.

44. Reynolds RW, Smith TM. A high-resolution global sea surface temperature climatology. Journal of Climate. 1995 Jun; 8(6):1571–83.

45. Reynolds RW, Rayner NA, Smith TM, Stokes DC, Wang W. An improved in situ and satellite SST analysis for climate. Journal of climate. 2002 Jul 1; 15(13):1609–25.

46. Reynolds RW, Chelton DB. Comparisons of daily sea surface temperature analyses for 2007–08. Journal of climate. 2010 Jul 1; 23(13):3545–62.

47. Reynolds RW, Chelton DB, Roberts-Jones J, Martin MJ, Menemenlis D, Merchant CJ. Objective determination of feature resolution in two sea surface temperature analyses. Journal of Climate. 2013 Apr 15; 26(8):2514–33.

48. Castillo KD, Lima FP. Comparison of in situ and satellite-derived (MODIS-Aqua/Terra) methods for assessing temperatures on coral reefs. Limnology and Oceanography: Methods. 2010 Mar; 8(3):107–17.

49. Liao E, Lu W, Yan XH, Jiang Y, Kidwell A. The coastal ocean response to the global warming acceleration and hiatus. Scientific reports. 2015 Nov 16; 5(1):1–0.

50. Langlais CE, Lenton A, Heron SF, Evenhuis C, Gupta AS, Brown JN, et al. Coral bleaching pathways under the control of regional temperature variability. Nature Climate Change. 2017 Nov; 7(11):839–44.

51. Seabra R, Varela R, Santos AM, Gomez-Gesteira M, Meneghesso C, Wethey DS, et al. Reduced nearshore warming associated with eastern boundary upwelling systems. Frontiers in Marine Science. 2019 Mar 8; 6:104.

52. Minnett PJ. Consequences of sea surface temperature variability on the validation and applications of satellite measurements. Journal of Geophysical Research: Oceans. 1991 Oct 15; 96(C10):18475–89.

53. Castillo KD, Lima FP. Comparison of in situ and satellite-derived (MODIS-Aqua/Terra) methods for assessing temperatures on coral reefs. Limnology and Oceanography: Methods. 2010 Mar; 8(3):107–17.

54. Smit AJ, Roberts M, Anderson RJ, Dufois F, Dudley SF, Bornman TG, et al. A coastal seawater temperature dataset for biogeographical studies: large biases between in situ and remotely-sensed data sets around the coast of South Africa. PLoS One. 2013 Dec 3; 8(12):e81944. https://doi.org/10.1371/journal.pone.0081944 PMID: 24312609

55. Brewin RJ, de Mora L, Billson O, Jackson T, Russell P, Brewin TG, et al. Evaluating operational AVHRR sea surface temperature data at the coastline using surfers. Estuarine, Coastal and Shelf Science. 2017 Sep 5; 196:276–89.

56. Thakur KK, Vanderstichel R, Barrell J, Stryhn H, Patanasatienkul T, Revie CW. Comparison of remotely-sensed sea surface temperature and salinity products with in situ measurements from British Columbia, Canada. Frontiers in Marine Science. 2018 Apr 6; 5:121.

57. Wick GA, Emery WJ, Schluessel P. A comprehensive comparison between satellite-measured skin and multichannel sea surface temperature. Journal of Geophysical Research: Oceans. 1992 Apr 15; 97 (C4):5569–95.

58. Smith T. M. and Reynolds R. W. (1998). A high-resolution global sea surface temperature climatology for the 1961–90 base period. Journal of Climate, 11(12), pp.3320–3323.

59. Reynolds RW, Rayner NA, Smith TM, Stokes DC, Wang W. An Improved In Situ and Satellite SST Analysis. InJ. Clim.

60. Chao Y, Li Z, Farrara JD, Hung P. Blending sea surface temperatures from multiple satellites and in situ observations for coastal oceans. Journal of atmospheric and oceanic technology. 2009 Jul; 26 (7):1415–26.

61. Schlegel RW, Oliver EC, Perkins-Kirkpatrick S, Kruger A, Smit AJ. Predominant atmospheric and oceanic patterns during coastal marine heatwaves. Frontiers in Marine Science. 2017 Oct 12; 4:323.

62. Bulgin CE, Embury O, Merchant CJ. Sampling uncertainty in gridded sea surface temperature products and Advanced Very High Resolution Radiometer (AVHRR) Global Area Coverage (GAC) data. Remote Sensing of Environment. 2016 May 1; 177:287–94.

63. Reynolds RW, Chelton DB, Roberts-Jones J, Martin MJ, Menemenlis D, Merchant CJ. Objective determination of feature resolution in two sea surface temperature analyses. Journal of Climate. 2013 Apr 15; 26(8):2514–33.

64. Hobday AJ, Alexander LV, Perkins SE, Smale DA, Straub SC, Oliver EC, et al. A hierarchical approach to defining marine heatwaves. Progress in Oceanography. 2016 Feb 1; 141:227–38.

65. Lourenço CR, Zardi GI, McQuaid CD, Serrao EA, Pearson GA, Jacinto R, et al. Upwelling areas as climate change refugia for the distribution and genetic diversity of a marine macroalga. Journal of biogeography. 2016 Aug; 43(8):1595–607.

66. Black BA, Schroeder ID, Sydeman WJ, Bograd SJ, Wells BK, Schwing FB. Winter and summer upwelling modes and their biological importance in the California Current Ecosystem. Global Change Biology. 2011 Aug; 17(8):2536–45.

67. Shannon LV, Nelson G. The Benguela: large scale features and processes and system variability. InThe south atlantic 1996 (pp. 163–210). Springer, Berlin, Heidelberg.

68. Pelegrí JL, Arístegui J, Cana L, González-Dávila M, Hernández-Guerra A, Hernández-León S, et al. Coupling between the open ocean and the coastal upwelling region off northwest Africa: water recirculation and offshore pumping of organic matter. Journal of Marine Systems. 2005 Feb 1; 54(1–4):3–7.

69. Meunier T, Barton ED, Barreiro B, Torres R. Upwelling filaments off Cap Blanc: Interaction of the NW African upwelling current and the Cape Verde frontal zone eddy field?. Journal of Geophysical Research: Oceans. 2012 Aug; 117(C8).

70. Bolton JJ. Marine phytogeography of the Benguela Upwelling region on the west coast of southern Africa: A temperature dependent approach. Botanica Marina. 1986 Jan 1; 29(3):251–6.

71. Farmer EC, Demenocal PB, Marchitto TM. Holocene and deglacial ocean temperature variability in the Benguela upwelling region: Implications for low-latitude atmospheric circulation. Paleoceanography. 2005 Jun; 20(2).

72. Tim N, Zorita E, Schwarzkopf FU, Rühs S, Emeis KC, Biastoch A. The impact of Agulhas leakage on the central water masses in the Benguela upwelling system from a high-resolution ocean simulation. Journal of Geophysical Research: Oceans. 2018 Dec; 123(12):9416–28.

73. Bachèlery ML, Illig S, Rouault M. Interannual coastal trapped waves in the Angola-Benguela upwelling system and Benguela Niño and Niña events. Journal of Marine Systems. 2020 Mar 1; 203:103262.

74. Hutchings L, Van der Lingen CD, Shannon LJ, Crawford RJ, Verheye HM, Bartholomae CH, et al. The Benguela Current: An ecosystem of four components. Progress in Oceanography. 2009 Dec 1; 83(1–4):15–32.

75. Schlegel RW, Smit AJ. Climate change in coastal waters: time series properties affecting trend estimation. Journal of Climate. 2016 Dec 15; 29(24):9113–24.

76. Nelson G, Hutchings L. The Benguela upwelling area. Progress in Oceanography. 1983 Jan 1; 12 (3):333–56.

77. Lutjeharms JR, Meeuwis JM. The extent and variability of South-East Atlantic upwelling. South African Journal of Marine Science. 1987 Jun 1; 5(1):51–62.

78. Shannon LV, Nelson G. The Benguela: large scale features and processes and system variability. In the South Atlantic 1996 (pp. 163–210). Springer, Berlin, Heidelberg.

79. Weeks SJ, Barlow R, Roy C, Shillington FA. Remotely sensed variability of temperature and chlorophyll in the southern Benguela: upwelling frequency and phytoplankton response. African Journal of Marine Science. 2006 Nov 1; 28(3–4):493–509.

80. Reynolds RW, Smith TM. A high-resolution global sea surface temperature climatology. Journal of Climate. 1995 Jun; 8(6):1571–83.

81. Banzon V, Smith TM, Chin TM, Liu C, Hankins W. A long-term record of blended satellite and in situ sea-surface temperature for climate monitoring, modeling and environmental studies. Earth System Science Data. 2016 Apr 28; 8(1):165–76.

82. Jury MR. Characteristics of summer wind fields and air-sea interactions over the Cape Peninsula upwelling region (Doctoral dissertation, University of Cape Town).

83. Schlegel RW, Smit AJ. heatwaveR: A central algorithm for the detection of heatwaves and cold-spells. Journal of Open Source Software. 2018 Jul 31; 3(27):821.

84. El Aouni A, Minaoui K, Tamim A, Daoudi K, Yahia H. An improved method for accurate computation of coastal upwelling index using sea surface temperature images. In2018 9th International Symposium on Signal, Image, Video and Communications (ISIVC) 2018 Nov 27 (pp. 76–81). IEEE.

85. Ricciardulli L, Wentz FJ. Uncertainties in sea surface temperature retrievals from space: Comparison of microwave and infrared observations from TRMM. Journal of Geophysical Research: Oceans. 2004 Dec; 109(C12).

86. Liu Y, Minnett PJ. Sampling errors in satellite-derived infrared sea-surface temperatures. Part I: Global and regional MODIS fields. Remote sensing of environment. 2016 May 1; 177:48–64.

87. Kilpatrick KA, Podesta GP, Evans R. Overview of the NOAA/NASA advanced very high resolution radiometer Pathfinder algorithm for sea surface temperature and associated matchup database. Journal of Geophysical Research: Oceans. 2001 May 15; 106(C5):9179–97.

88. Dufois F, Penven P, Whittle CP, Veitch J. On the warm nearshore bias in Pathfinder monthly SST products over Eastern Boundary Upwelling Systems. Ocean Modelling. 2012 Jan 1; 47:113–8.

89. Donlon CJ, Martin M, Stark J, Roberts-Jones J, Fiedler E, Wimmer W. The operational sea surface temperature and sea ice analysis (OSTIA) system. Remote Sensing of Environment. 2012 Jan 15; 116:140–58.

90. Tittensor DP, Mora C, Jetz W, Lotze HK, Ricard D, Berghe EV, et al. Global patterns and predictors of marine biodiversity across taxa. Nature. 2010 Aug; 466(7310):1098–101. https://doi.org/10.1038/nature09329 PMID: 20668450

91. Duncan MI, James NC, Bates AE, Goschen WS, Potts WM. Localised intermittent upwelling intensity has increased along South Africa's south coast due to El Niño–Southern Oscillation phase state. African Journal of Marine Science. 2019 Oct 7; 41(3):325–30.

92. Sawall Y, Harris M, Lebrato M, Wall M, Feng EY. Discrete pulses of cooler deep water can decelerate coral bleaching during thermal stress: Implications for artificial upwelling during heat stress events. Frontiers in Marine Science. 2020 Aug 28; 7:720.

93. Wang D, Gouhier TC, Menge BA, Ganguly AR. Intensification and spatial homogenization of coastal upwelling under climate change. Nature. 2015 Feb; 518(7539):390–4. https://doi.org/10.1038/nature14235 PMID: 25693571

94. Iles AC, Gouhier TC, Menge BA, Stewart JS, Haupt AJ, Lynch MC. Climate-driven trends and ecological implications of event-scale upwelling in the C alifornia C urrent S ystem. Global Change Biology. 2012 Feb; 18(2):783–96.

95. Currie R. Upwelling in the Benguela current.

96. Hart TJ, Currie RI. The Benguela Current. University Press; 1960.

97. Broitman BR, Mieszkowska N, Helmuth B, Blanchette CA. Climate and recruitment of rocky shore intertidal invertebrates in the eastern North Atlantic. Ecology. 2008 Nov; 89(sp11):S81–90. https://doi.org/10.1890/08-0635.1 PMID: 19097486

98. Minnett PJ. Consequences of sea surface temperature variability on the validation and applications of satellite measurements. Journal of Geophysical Research: Oceans. 1991 Oct 15; 96(C10):18475–89.